

Role of Atomic Physics in Models for Enhanced Edge Transport

J. Hogan

ORNL Fusion Energy Division, Oak Ridge, TN 37830

Abstract. Since regulation of helium ash accumulation in future magnetic confinement D-T burning plasma experiments requires control of recycling helium, the quest for improved magnetic confinement performance leads to a paradoxical necessity to degrade some confinement properties selectively in the plasma edge. This paper describes the role of atomic and molecular data in current models for several proposed ways to do this: 'Type I ELM-y H-mode', the ergodic divertor, and enhanced radiation operational modes. The same constraint requires better control of intrinsic impurities. The use of atomic and molecular data in the comparison of intrinsic impurity generation rates with observation is also illustrated.

INTRODUCTION

Burn requirements for D-T magnetic confinement plasmas impose a strong need for control of the accumulation of α -particle reaction products. The problem is made acute by the fact that helium ash preferentially recycles back to the core plasma and thus must be actively exhausted. D-T ignition typically requires a low value of the relevant figure-of-merit, $\tau_{He^*} / E < 10$ (τ_{He^*} is the helium residence time in the plasma, and E is the energy confinement time) [1]. Since fusion device design typically maximizes E , lowering the value of τ_{He^*} is the best available route to achieve this. The helium residence time, $\tau_{He^*} = \tau_{He} + \tau_{He}^{edge} / (1-R_{He})$, where τ_{He} is the confinement time in the plasma core of the original fusion-produced α s, τ_{He}^{edge} is the characteristic residence time for helium subsequently re-cycled at the edge, and R_{He} is the helium recycling probability. Given present exhaust capabilities, $R_{He} \sim 1$, so there is a strong incentive to reduce τ_{He}^{edge} as much as possible while maintaining high core confinement. Species-selective degradation of edge confinement for helium alone is not yet practical, so general edge confinement degradation is indicated.

The ELMy H-mode (Edge Localized Mode High confinement mode) operational scenario for future burning plasma experiments does just this. Periodic instability bursts at a fixed edge spatial location expel edge plasma and leave the core plasma relatively unchanged [2]. A complementary scheme, explored on the Tore Supra tokamak, introduces static edge-localized magnetic perturbations with 3-D spatial modulation, to selectively degrade edge particle confinement [3, 4]. However, any degradation of edge confinement strongly increases the heat efflux, so attempts have been made to reduce the heat flux burden by increasing edge radiation through

injection of extrinsic impurities, such as neon and argon, to produce Radiatively-Improved (or RI) modes. [5]. However, the ignition requirement for n_{He^*} / n_e is made much more stringent when these, and also intrinsic impurities (mainly carbon in present devices) are included [6]. Thus, increased attention is being given to identifying the sources of intrinsic impurities and reducing them.

Examples illustrating the application of atomic and molecular data in current studies of edge optimization are described.

ELMY H-MODE IMPURITY DYNAMICS

Helium exhaust is facilitated by increased enrichment of the helium concentration in the divertor relative to that in the core plasma. (enrichment $= c^{core} / c^{div}$, where c is the helium relative concentration). An impurity dynamics simulation using the solps4.0 version of the b2-Eirene code [7] illustrates the enrichment process during an ELM event for neon, chosen for similarity to helium. The code couples a 2-D fluid plasma model (b2) with a 2-D neutrals code (Eirene) to make a time-dependent simulation of ELM behavior for a DIII-D lower single-null divertor case. Periodic ELM events are modeled by enhancing the electron and ion radial diffusivity five-fold during a 100 μ sec interval, at the experimentally observed frequency. Figure 1 shows the magnetic geometry of the region modeled, near the DIII-D lower, outer baffle, and also shows a snap-shot of the deuterium neutral density near its maximum. Figure 2 shows the evolution of the divertor electron temperature (T_e^{div}) and of the total neon ion density through one ELM period. For each ELM there is a temperature crash just after ELM onset which produces $T_e^{div} \approx 1$ eV and a detached strike point (low-or zero-current to the divertor plates). T_e^{div} then recovers and rises until the next crash and, during the recovery phase, the plasma is attached. Since T_e^{div} can drop below the ionization potential for NeI at the outset of the ELM cycle, the neon ion density also crashes at first, and then, as T_e^{div} rises, neon is re-ionized after having been dispersed throughout the region. During the ELM recovery phase considerable neon recycling from the front face of the baffle is shown, due to the prior dispersal of neon during the detached phase. The dispersal, and concomitant redirection of recycling from the divertor plate (where pumping is optimal) to other surfaces acts to reduce the enrichment. Because of the large deuterium neutral density at during the detached phase (Fig. 1) this situation raises the possibility that ion dynamics may be strongly affected by deuterium charge exchange with neon ions. As shown in Fig. 3 (time-independent calculations with the b2 divertor code) there is a strong sensitivity of expected enrichment to variation in the charge exchange rate. Present modeling calculations for neon adopt the general scaling $R_{cx} = 2 \cdot 10^{-15} Z^{1.14} T_i^{0.35}$ [8] for deuterium charge exchange with ions of charge Z . Better (species-specific) charge exchange rates would improve the simulation. Much previous spectroscopic data has been obtained only after averaging over several ELM events. Since data with better time resolution are becoming available, the model comparison and validation should be improved in the near future, but until the basic processes governing enrichment can be better quantified, predictive capability will remain limited.

ERGODIC DIVERTOR IMPURITY TRANSPORT

Ergodic divertor experiments in Tore Supra have also demonstrated an edge impurity regulation effect [4]. The static edge confinement degradation due to ergodic magnetic perturbations has been examined in two cases in which neon spatial profiles were measured. The profiles were obtained with a grazing incidence VUV duochromator with a vibrating mirror in the spectrometer line of sight which measures spatial (poloidal) profiles of the impurity emission lines for the lower half of the Tore Supra plasma [9]. The duochromator finds a complex signal, with the usual (Abel-invertable) peak near the tangency radius where the chords intersect the plasma flux surface with the peak density of the ion in question, but also a second prominent peak near the equator. Figure 4 (curve 'DATA') schematically illustrates the situation. It is found that by augmenting the Abel-invertable symmetric radial shell of emitting ions with an additional component due to localized recycling from the face of the nearby outboard pump limiter, a reasonable quantitative model for the duochromator signal can be constructed [10]. The MIST radial impurity transport code [11] has been used to calculate the poloidally symmetric contribution to the duochromator signal. The asymmetric (limiter) contribution is modeled with the 3-D BBQ scrape-off layer transport code [12]. The model for the profile uses recently developed excitation rates for neon ions [13] allowing discrimination between the behavior of T_e -sensitive ($n=1$) and T_e -insensitive ($n=0$) emission. In addition to these rates, used for NeVII and VIII, the empirical $n=0$ excitation rates from [14] have been used for NeIV and NeV ions. Using measured radial profiles of n_e and T_e , the expected duochromator signal is modeled. Figure 5 (a-d) shows the resulting match between the BBQ/MIST model and the data for Ne IV, V, VII and VIII. The composite model has been able to provide both a qualitative (as shown in Fig. 4.) and, when used with a transport model developed for the ergodic divertor conditions (next section), a quantitative prediction of the duochromator signal

The ergodic divertor also induces systematic poloidal modulations observed by the duochromator when the plasma is removed from contact with the outboard limiter and instead placed in contact with the inner wall. In this case results from the composite model (axisymmetric core and non-symmetric edge contributions) shows that, in addition to the expected direct effect of T_e modulations arising from the laminar field of the ergodic divertor, there is also strong evidence for the effect of impurity charge exchange. The inner-wall limited configuration gives rise to significant neutral density in the observation zone. The level of neutral density is estimated with respect to previous measurements made near the divertor neutralizer [15], using results from a deuterium collisional-radiative model [16]. Using this estimate for the neutral deuterium density and the previously cited charge-exchange reaction scaling laws [8], the modulations in the poloidal profiles are found to agree with observation [17].

ENHANCED EDGE RADIATION MODES

Injection of selected high-recycling impurities (typically neon and argon) has been pursued to reduce the heat flux while maintaining high core confinement. Tore Supra experiments have been carried out to compare the added radiation arising from injection of extrinsic neon and argon impurities with that in the case of nitrogen, which is efficiently pumped. Modeling of this experiment with the combined edge (BBQ) and core (MIST) codes shows that the model gives a reasonable description for the enhanced edge transport under ergodic divertor conditions. In this case treatment of the influx of impurities into the core plasma as ions, rather than as a neutral influx, as is the conventionally assumed, plays a key role in calculation of the radiated power. The core impurity code models the evolution of the flux-surface averaged impurity density in terms of the flux-surface averaged radial diffusion equation

$$\frac{\partial n_{zi}}{\partial t} + \frac{1}{\rho} \frac{\partial}{\partial \rho} (\rho \Gamma_{zi}) = S_{zi} \quad \text{with} \quad \Gamma_{zi} = -D_A(\rho) \frac{\partial n_{zi}}{\partial \rho} + V_A(\rho) n_{zi}$$

where Γ_{zi} is the impurity radial flux density for species i , ρ is the normalized radius (in toroidal flux coordinates), S_{zi} is the local source of species i , and D_A and V_A are the anomalous diffusivity and radial convective velocity. The source term $S_{zi}(\rho)$ represents the local source of ions with charge Z_i arising through local ionization and recombination processes and also through direct influx at radius ρ from transport processes in the ergodic layer.

Core impurity transport rates have been determined from cases for which charge-exchange recombination radial profiles were measured at full ergodic divertor strength [18], and these provide local radial impurity transport coefficients, $D_A(\rho)$, $V_A(\rho)$. Radiative efficiencies are compared for comparable scenarios with 45 kA divertor current and application of 4 MW ICRH power, followed by a short impurity injection pulse. The total radiative power for carbon, oxygen and the relevant extrinsic impurity is calculated from the model. For the case of neon, the rates are taken from the ADAS database [19]. [adf11/plt/pl91_ne.dat with updates by R. Dux (IPP-Garching)]. Nitrogen radiation is calculated using the ADPAK atomic physics data from the MIST code and argon rates are based on the STRAHL model [20] and including modifications from HULLAC [21]. In each case the background carbon and oxygen content is fit prior to the application of ICRH heating, using the Z_{eff} increase to help determine the isotopic composition between carbon and oxygen. Figure 6 shows the comparison of modeled total radiative loss and that measured by the Tore Supra horizontal bolometer for the cases of Ne, N and Ar injection. A comparison of radiative efficiency (maximum radiated power density / impurity density at the position of maximum radiation density) shows that Ar is the most effective radiator ($\sim 1.6 - 2.3 \cdot 10^{-11}$ W / particle), and that N and Ne have smaller and comparable values ($\sim 0.9 \cdot 10^{-11}$ W/particle).

INTRINSIC IMPURITY SOURCES

The identification of intrinsic impurity sources is complicated by transient behavior (ELM activity) in likely scenarios. Further, most current machines rely on non-cooled plasma-facing components, so that an initially small, localized hot spot will grow in magnitude as the discharge continues. Spectroscopic observation, typically integrated over several ELMs, has been used to make a first characterization of sources. The identification of characteristic CD and C₂ band emission is used to distinguish chemical (former) and physical (latter) graphite erosion processes. The measurement of molecular rotational temperature is a further clue. For this problem the recent improvement of rate databases for break-up of complex hydrocarbons [18, 19] has advanced modeling capability. Fig. 7 shows a calculation from the BBQ Monte Carlo impurity transport code[12] of the break-up process for acetylene (C₂D₂) originating at a simulated hot spot in the DIII-D device. Molecular spectroscopy finds carbon molecular temperatures to be in the range of 0.1 eV [20]. Simulating the break-up process beginning with a neutral C₂D₂ source, the calculation finds that, while molecular temperatures vary up to 1 eV in the observation volume, the density-weighted temperature is 0.1 - 0.3 eV, which is in the measured range. However, there is still substantial uncertainty in the rates used in modeling the evolution of hydrocarbon erosion products, and this is an area where improved molecular data would be quite helpful.

CONCLUSIONS

The increased fuel particle and impurity efflux resulting from edge confinement optimization seems to lead inexorably to a condition in which impurity charge exchange with deuterium will be important. For modeling of ELMs and the ergodic divertor charge exchange between low energy deuterium neutrals and partially ionized noble gases, such as neon and argon, is observed to be an important aspect. At present modeling codes employ rather crude scaling relations for these rates, so that species-resolved charge exchange rates for recycling impurities such as neon and argon would be of great benefit. Although recent results for emissivities of these ions have proven quite useful, the radiative rates which are used in modeling RI-mode evolution are still qualitative. In the study of intrinsic impurity sources, the availability of improved rate data for breakup of complex hydrocarbons has enabled better understanding of generation processes. However, there are a great many reaction pathways and the opportunities for direct validation of the rates in the plasma environment are limited.

ACKNOWLEDGMENTS

Supported by the U.S. DOE under contract No. DE-AC05-00OR22725 with UT-Battelle, LLC.

REFERENCES

1. Reiter, D., Wolf, G.H., Keve H, *Nuclear Fusion* **30** (1990) 2141
2. Wagner, F., Becker, G., Behringer, K. et al. et al, *Phys.Rev. Letters* **49**, (1982) 1408
3. Feneberg, G. and Wolf, G.H *Nucl. Fusion*, **21** 669 (1981)
4. Samain, A., Grosman, A., Belnski, T., et al *J. Nucl. Mater.* **128&129** (1984) 395
5. Messiaen, A., et al *Nuclear Fusion* **36** (1996) 39
6. Samm, U., Tokar', M.Z., Unterberg, B., 22nd EPS
(EPS, Bournemouth, UK, 1995), vol. 19C II-201-204.
7. Schneider, R., Reiter, D., Zehrfeld, H.P. et al *J. Nucl. Mater.* **196&198** (1992) 810
8. Piuatti, M-E., et al *Plasma Physics*, **23** (1981) 1075
9. Breton, C., De Michelis, C., Finkenthal, M., Mattioli, M., *J. Phys. E: Sci. Instrum.* **12** (1979) 894
10. Hulse, R., *Fus. Technol.* **3** (1983) 259
11. Hogan, J., De Michelis, C., Monier-Garbet, P., et al. *J. Nucl. Mater.* **290-293** (2001) 628
12. Hogan, J., Klepper, C., Harris, J, 16th Intern. Conf. Plasma Physics Controlled Nuclear Fusion
Research (Montreal, 1996), IAEA: Vienna, **2** 625
13. Fournier, K., Mattioli, M. et al, *Phys. Rev. E* **60** (1999) 4760
14. Mewe, R., Schrijver, J. and Sylwester J., *Astron. Astrophys.*, **87** (1980) 55
15. Escarguel, A., Pegourie, B., Hogan, J. et al ., et al *Plasma Phys Control. Fusion*, **43** (2001) 1733
16. Fujimoto, T., Sawada, K., Takahata, K., *J. Appl. Phys.* **66** (1989) 2315, Sawada, K., Eriguchi, K.,
Fujimoto, T., *J. Appl. Phys.* **73** (1993) 8122, Sawada, K., Fujimoto, T., *J. Appl. Phys.* **78** (1995)
2913
17. Hogan, J., De Michelis, C., Monier-Garbet, P., *Plas. Phys. Control. Fus.* (to be published)
18. Hess, W., Farjon J.L., Guirlet R., Druetta M. *Rev. Sci. Instrum.* (to to be published)
19. Summers, H.P., Atomic Data and Analysis Structure (ADAS), Report JET-IR(94)06 (1994) JET
Joint Undertaking, Abingdon (England); ADAS User Manual, version 2.2 2000
20. Behringer, K., et al *Plas. Phys. Control. Fus.* **31** (1989) 2059
21. Mattioli, M., Fournier, K., Piuatti, M E et al *Plas. Phys. Control. Fus.* **44** (2002) 33
22. Allman, D., Ruzik, D., Brooks, J., et al *Phys. Plas.* **7** (2000) 1421
23. Janev, R.K. et al "Cross sections and rate coefficients for electron-impact ionization of hydrocarbon
molecules", NIFS-DATA-68, Oct. 2001, National Institute for Fusion Science, Japan
24. Isler, R.C., Colchin, R., Brooks, N. et al et al *Phys. Plas.* (to be published)

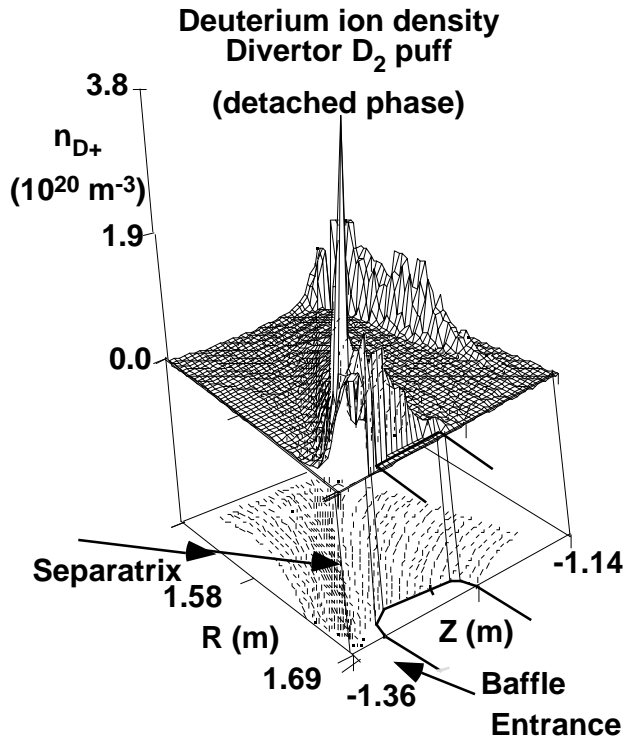


FIGURE 1 Magnetic geometry near DIII-D baffle, deuterium density at its maximum value in time.

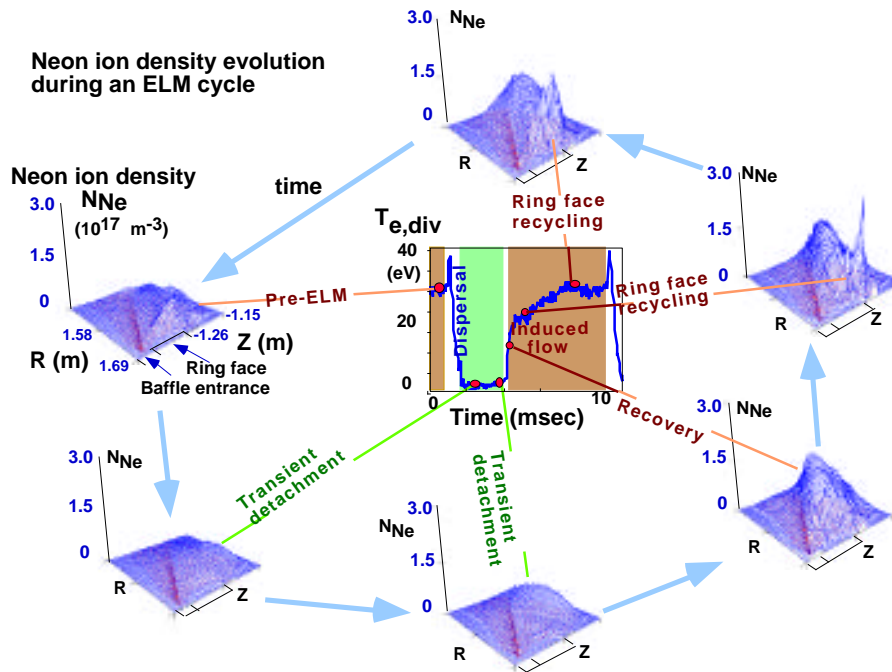


FIGURE 2. Neon ion ELM cycle dynamics simulation with solps4.0 (b2-Eirene code)

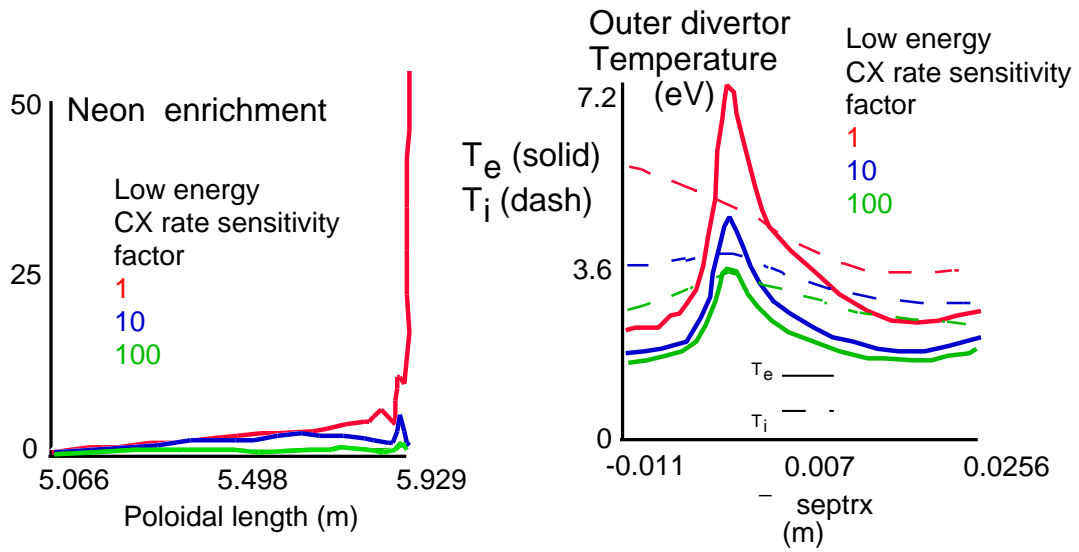


FIGURE 3. Sensitivity of enrichment (function of parallel length) and divertor T_e (vs major radius) To deuterium CX rate.

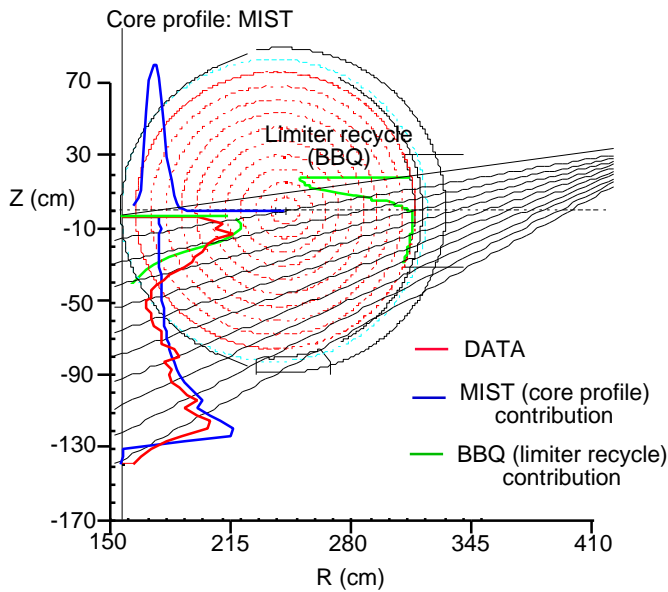


FIGURE 4. Schematic view of Tore Supra VUV duochromator poloidal profile measurement. Data profile is compared with contributions from symmetric ('MIST') and asymmetric ('BBQ') sources.

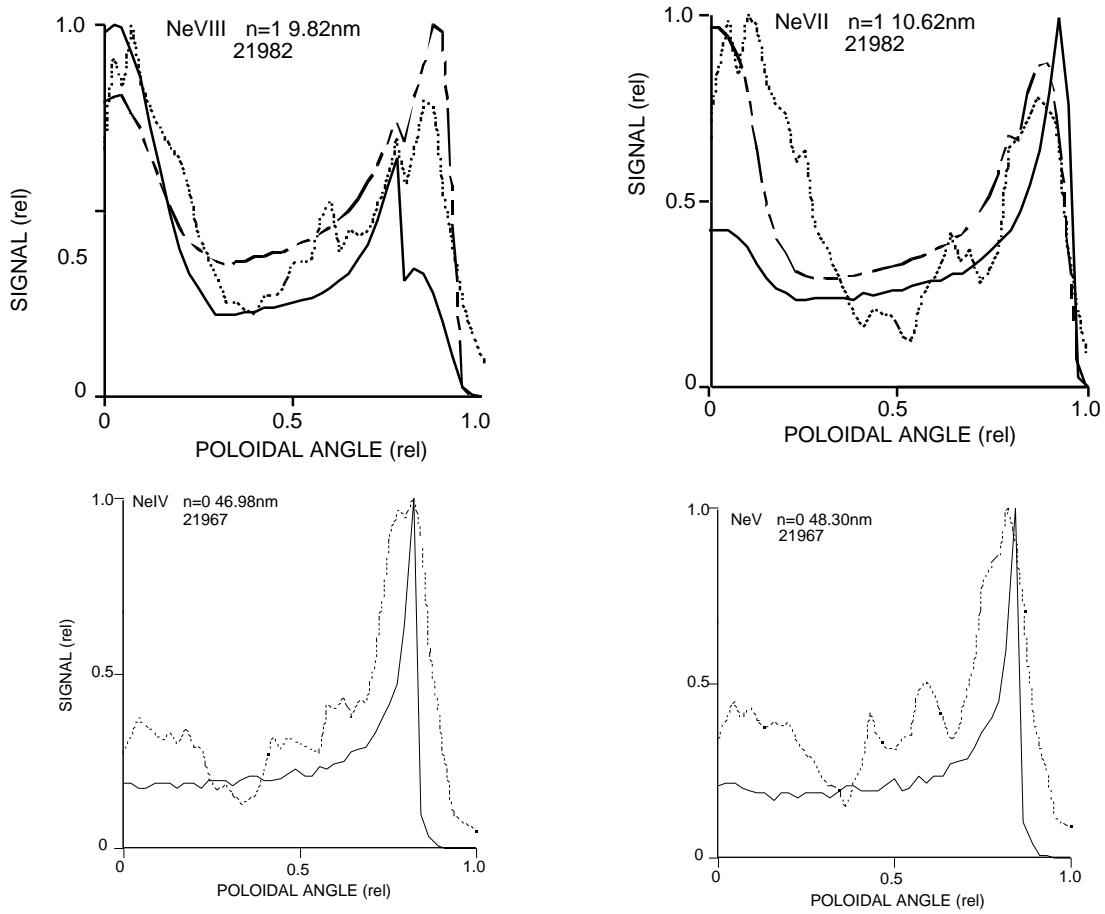


FIGURE 5. Comparison of measured duochromator profiles for NeIV, NV ($n=0$), NeVII, NeVIII ($n=1$) with results from composite model.

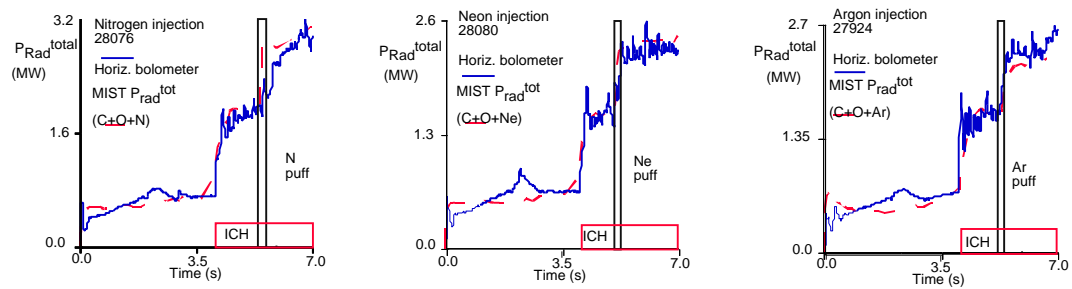


FIGURE 6. Comparison of radiated power calculated from the composite model with Tore Supra horizontal bolometer measurements.

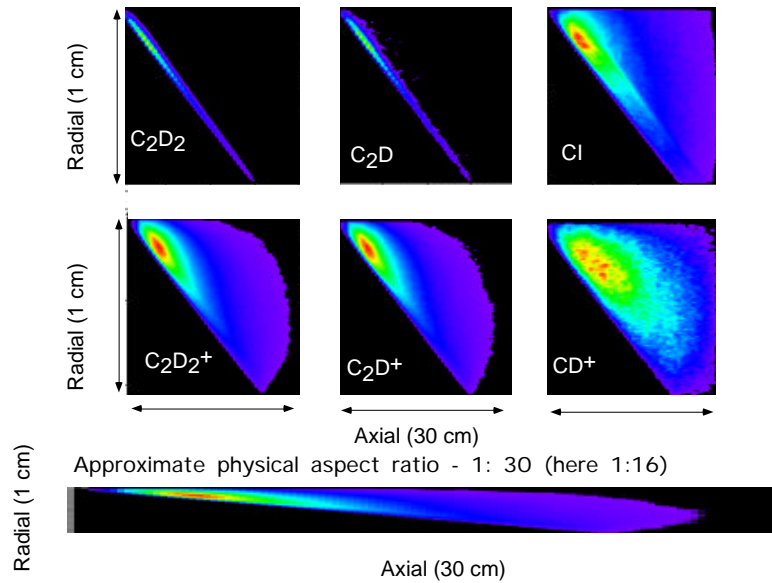


FIGURE 7 . Density of C_2D_2 break-up products originating at a simulated hot spot, calculated with the BBQ code.

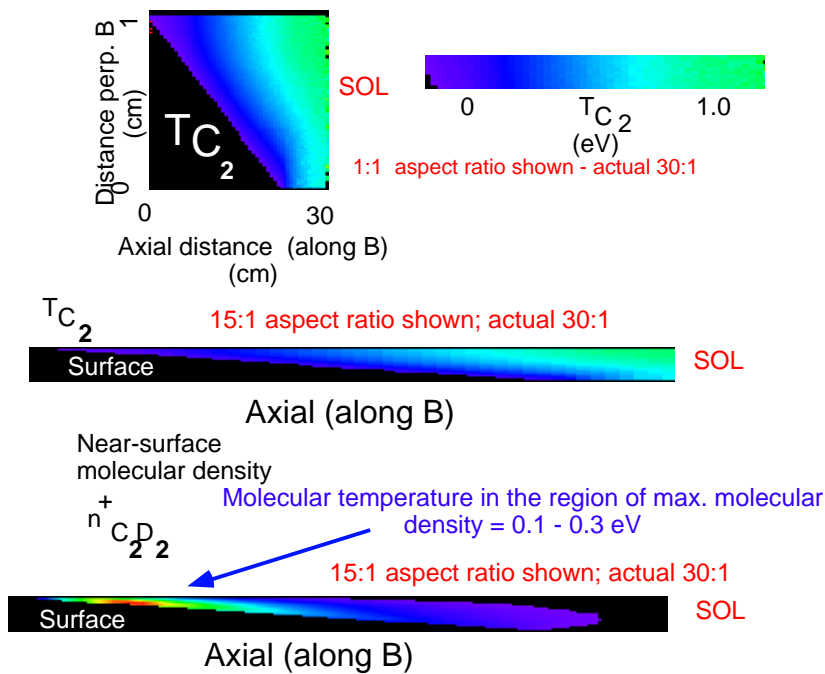


FIGURE 8. BBQ calculation of carbon molecular temperature